

INTERACTION OF RADIATION WITH MATTER https://doi.org/10.1070/QEL17449

Comparative study of the dynamics of laser breakdown in water and hexane using interference microscopy

V.V. Kononenko, V.M. Gololobov, T.V. Kononenko, E.A. Goncharov, V.I. Konov

Abstract. **The changes in the optical properties of water and hexane under femtosecond irradiation (Ti:Al_2O_3 laser, wavelength 800 nm, intensity $\sim 10^{13}$ W cm^{-2}) are investigated in the cavitation (bubble-formation) regime using interference microscopy in a time interval of ~1.5 ns since the impact onset. A comparison of the dynamics of radiation-induced processes (solvation of excess electrons, pair recombination, and development of precavitation processes) is performed. The excited-carrier concentration is estimated, and these estimates are found to be inconsistent with the amount of energy that must be transferred to the liquid during a pulse to implement its heating and subsequent cavitation. This inconsistency is especially pronounced for hexane, where ionisation processes can barely be detected by interferometry. The experimental results put new questions about the mechanisms of energy transfer in both polar and nonpolar liquids subjected to intense laser irradiation.**

Keywords: *femtosecond laser radiation, laser-stimulated processes in liquids, interference microscopy.*

1. Introduction

Interference methods have successfully been used for a long time to study the processes induced in different media subjected to intense laser irradiation [1]. The well-developed approaches provide contactless measurement of the optical properties of a medium in the impact zone, and their combination with the probe measurement technique allows one to trace the dynamics of these changes. In this case, an extremely high resolution can be obtained in practice: The spatial resolution is as high as several tenths of micrometer, and the temporal resolution, determined by the duration of optical pulses in use, amounts to ~100 fs in modern measurement systems.

To date, interferometry has provided some important results describing the mechanisms of radiation absorption and its interaction with a perturbed medium, mechanisms of carrier thermalisation and recombination, and mechanisms of reversible and irreversible structural changes in irradiated media. The aforementioned studies were performed mainly in gases and solids [2–7]. Note that the first interference studies of laser-induced processes in liquids were performed a fairly long time ago [8], and a certain amount of experimental material has been accumulated to date [9, 10]. However, the exceptional and long-term interest in liquids calls for new various experimental methods capable of supplementing conventional ones: optical spectroscopy [11–15], photoelectron spectroscopy [16, 17], etc.

This interest is related to a series of promising applications in such fields as chemistry of solutions, molecular engineering of novel materials, impacts on biosystems at the cellular and molecular levels, etc. [18–21]. Undoubtedly, the main attention is paid to water as the most widespread liquid; at the same time, a great number of studies were devoted to other liquid compounds.

To date, it has become clear that the interaction of liquids with strong pulses is a more complex process than the corresponding interaction of gases and solids. A process common for all transparent media is nonlinear absorption, i.e. a key mechanism allowing for energy transfer (at a level of several electronvolts) to a molecular bond and thus making the molecule ionised. At a high peak intensity of focused femtosecond radiation (more than 10^{12} W cm^{-2}), this ionisation becomes dominant (in comparison with resonance excitation) and fairly intense (the concentration of ionised atoms becomes comparable with the total atomic concentration).

The main factor complicating the interaction for both polar and nonpolar liquids is that excitation of the electron subsystem of a liquid initiates a chain of fast processes of solvation and chemical-reaction nature. As a result, many various components arise (solvated electrons, parent ions, radicals and other fragments of polyatomic molecules, secondary products, etc. [22]), which affect significantly the optical properties and, therefore, the mechanisms of interaction with the pulse trailing edge. One of the fastest processes is the transformation of detached electron to the presolvated state and then to the solvated state. This transformation takes from 0.05 to 0.5 ps in water [11–13]. The modern knowledge about the interaction of a strong optical field with such a complex system as a charge in a strong solvent is highly limited. In this context, laser ionisation of liquids (in particular, water) remains a poorly predictable process (as compared with solids and gases).

In this paper, we report the results of a comparative study of the dynamics of changes in the optical properties of water and hexane exposed to intense femtosecond IR radiation. Hexane (C_6H_{14}), which belongs to the family of alkanes (saturated hydrocarbons), is, in contrast to water, a nonpolar liquid. Measurements were performed in the cavitation regime, i.e., using energies at which bubble formation occurs in the irradiated region; this process is caused by both heating the

V.V. Kononenko, V.M. Gololobov, T.V. Kononenko, E.A. Goncharov, V.I. Konov Prokhorov General Physics Institute of the Russian Academy of Sciences, 119991 Moscow, Russia;
e-mail: vitali.kononenko@nsc.gpi.ru

Received 24 September 2020; revision received 10 November 2020
Kvantovaya Elektronika **51** (2) 169–174 (2021)
Translated by Yu.P. Sin'kov

liquid (~150 °C for water) and the negative pressure developing in the course of time in the breakdown zone [18, 23].

2. Experimental

Experiments were performed with deionised double-distilled water (resistivity ~19 MΩ m at room temperature). Hexane (Acres Organics, 99% purity) was used without any additional treatment. A schematic of the experimental setup is presented in Fig. 1. A fused silica cell (10×10 mm) filled with a liquid under study was irradiated by a pulsed Ti:sapphire laser (wavelength 800 nm, pulse FWHM 135 fs). The laser beam was focused by an aspherical lens with a focal length of 30 mm into the cell near its front wall (the focusing depth was ~0.3 mm). The energy was varied in the range of 0.1–0.5 μJ.

A wide probe beam passed through a delay line (from 0 fs to 1.5 ns) and then through the liquid-containing cell, being oriented perpendicular to the pump beam. The local change in the refractive indices (n) and absorption (A), induced by intense radiation in the impact zone, led to modulation of the amplitude and phase of probe beam field (Fig. 1, inset I). An objective (NA = 0.40) and a lens (f = 500 mm), forming a telescope, were used to obtain an image of the impact zone on a CCD array. The parallel beam from the telescope passed through a Sagnac interferometer, whose mirrors were tuned so as to form a broadband interference pattern. The phase difference for the beams in the interferometer arms was set to be π/2, because in this case the interference is maximally sensitive to phase variation, and the interference pattern brightness is $B = (B_{max} + B_{min})/2$, where B_{max} and B_{min} are brightnesses for constructive and destructive interferences, respectively.

Inset II in Fig. 1 shows schematically two images of the excited region, which arise at a transverse displacement of beams in the interferometer arms and are fixed by the CCD array. Actually, these images are the result of interference of the unperturbed part of the wavefront of one beam with the perturbed part of the wavefront of the other beam. Correspondingly, as can be seen from the scheme of optical-field summation (Fig. 1), the probe-beam phase shift $\Delta\phi$ caused by laser excitation manifested itself as changes in the brightness of both images; note that these changes had opposite signs. At the same change in phase, one image became darker than the surrounding background, while the other became brighter. The phase shift was reconstructed independently for each image from the measured brightness. A detailed description of the reconstruction algorithm, including the formulas for $\Delta\phi$, can be found in [24]. The transmittance T of excited water, which is necessary to calculate $\Delta\phi$, was found from the shadow images that were formed when introducing a two-sided mirror into the interferometer (Fig. 1). Note that, with correct focusing of the projection objective; absorption taken into account; and exact measurement of the B, B_{max}, B_{min}, and other necessary parameters, the calculated phases for the two images differed by less than 10% in the entire range of probe-beam delays.

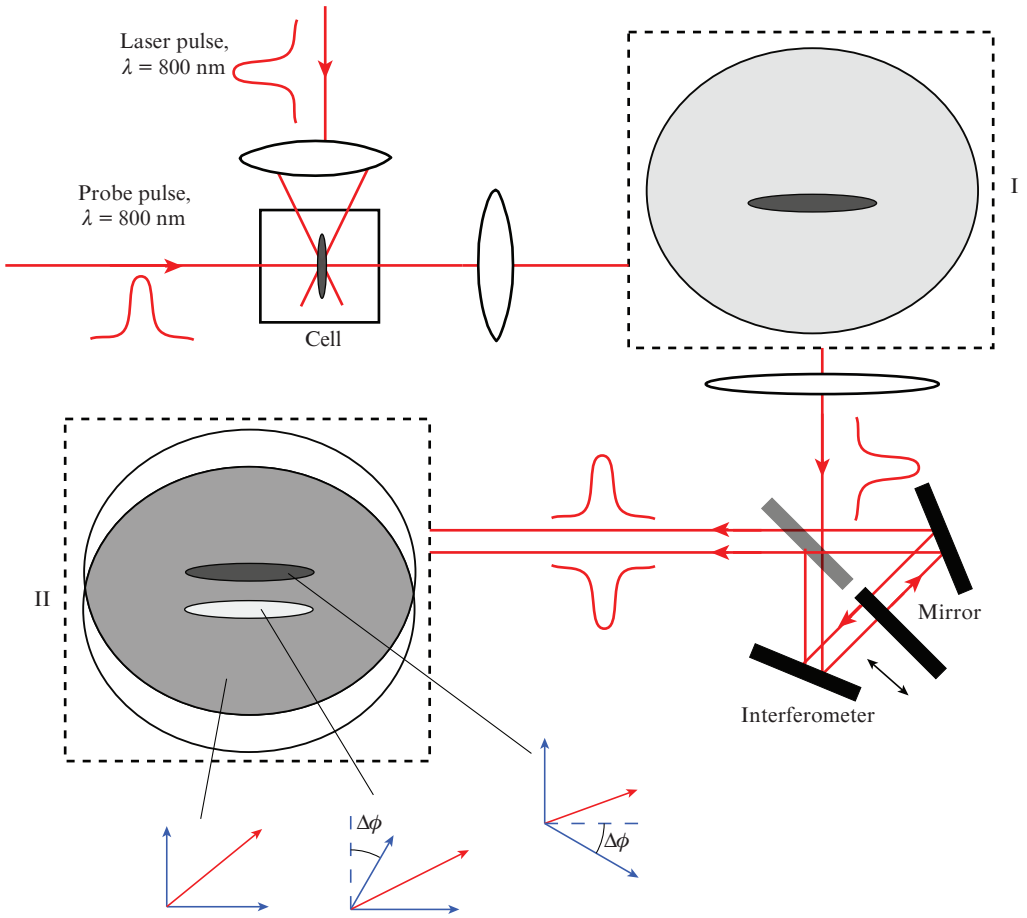

Figure 1. Setup for measuring the dynamics of the optical properties of a medium excited by intense femtosecond radiation (top) and a schematic clarifying the summation of optical fields in the interferometer (bottom).

The averaged $\Delta\phi$ value was used to analyse the dynamics of radiation-initiated processes. Note that such interference schemes do not make it possible to determine the sign of the phase shift in the probe beam and, correspondingly, the sign of the change in the refractive index of the medium, induced as a result of irradiation. The sign of $\Delta\phi$ in the dependences presented below was chosen proceeding from the physical interpretation of the observed dynamics of optical properties of liquids after their irradiation.

3. Results and discussion

Figure 2 shows distributions of the phase shift $\Delta\phi$ of the probe beam wavefront for a series of delays in the case of water irradiated by pulses with different energies E. At $E \lesssim 0.3$ μJ, perturbation of the medium manifested itself only when a pulse passed through the caustic (Fig. 2a). No plasma was observed in the impact zone. The visible white cloud moving with a speed of light is a manifestation of the optical Kerr effect, which leads to a local increase in the refractive index. Since this parameter is proportional to the radiation intensity, the observed hyperpolarisability can be used to reconstruct the parameters of a wave packet when the latter passes through the caustic. Under focusing conditions in use, the beam in water retained a Gaussian profile with a radius $r_g \approx 2$ μm (at the level of 1/e) and pulse duration $\tau_w \approx 160$ fs (at half maximum).

A pronounced plasma wake is observed for a pulse with an energy of 0.4 μJ (Fig. 2b), which corresponds (at $r_g \approx 2$ μm) to a laser fluence of ~ 3 J cm^{-2}. The presented images illustrate the key instants of the processes of laser excitation and subsequent water relaxation. White and black regions correspond, respectively, to increase ($+\Delta n$) and decrease ($-\Delta n$) in the refractive index.

The three upper panels in Fig. 2 fix the instants when the laser pulse is located in the beam waist, whose centre corresponds approximately to the observation region centre. A comparison of the interference patterns for pulses with different energies shows that in the presence of plasma the wave packet is visually decomposed into two parts: leading (A) and trailing (B) (Fig. 2b). At a delay of 99 fs, only the leading part fell in the field of view; due to the optical Kerr effect, it manifested itself as an increase in the polarizability of medium ($+\Delta n$). At a delay of 286 fs the pulse was located at the caustic centre, and its maximum corresponded to a negative change in polarisability ($-\Delta n$), which was interpreted as a result of water ionisation and occurrence of the so-called previously hydrated (wet) electrons [12]. The latter are weakly localised, and the maximum of their absorption lies in the IR range [14]; thus, under normal dispersion conditions, the polarisability at a wavelength of 800 nm must be negative. The trailing part of the pulse was most pronounced in all interference patterns: the polarisability of the medium in the spatial region occupied by it exceeded greatly the Kerr hyperpolarisability in unionised water (in the leading part). This jump ($+\Delta n$) disappeared 'instantaneously' when the laser field was switched off. As a result, the bright trailing part of the pulse was well-localised and moved through the caustic (as well as the leading part)

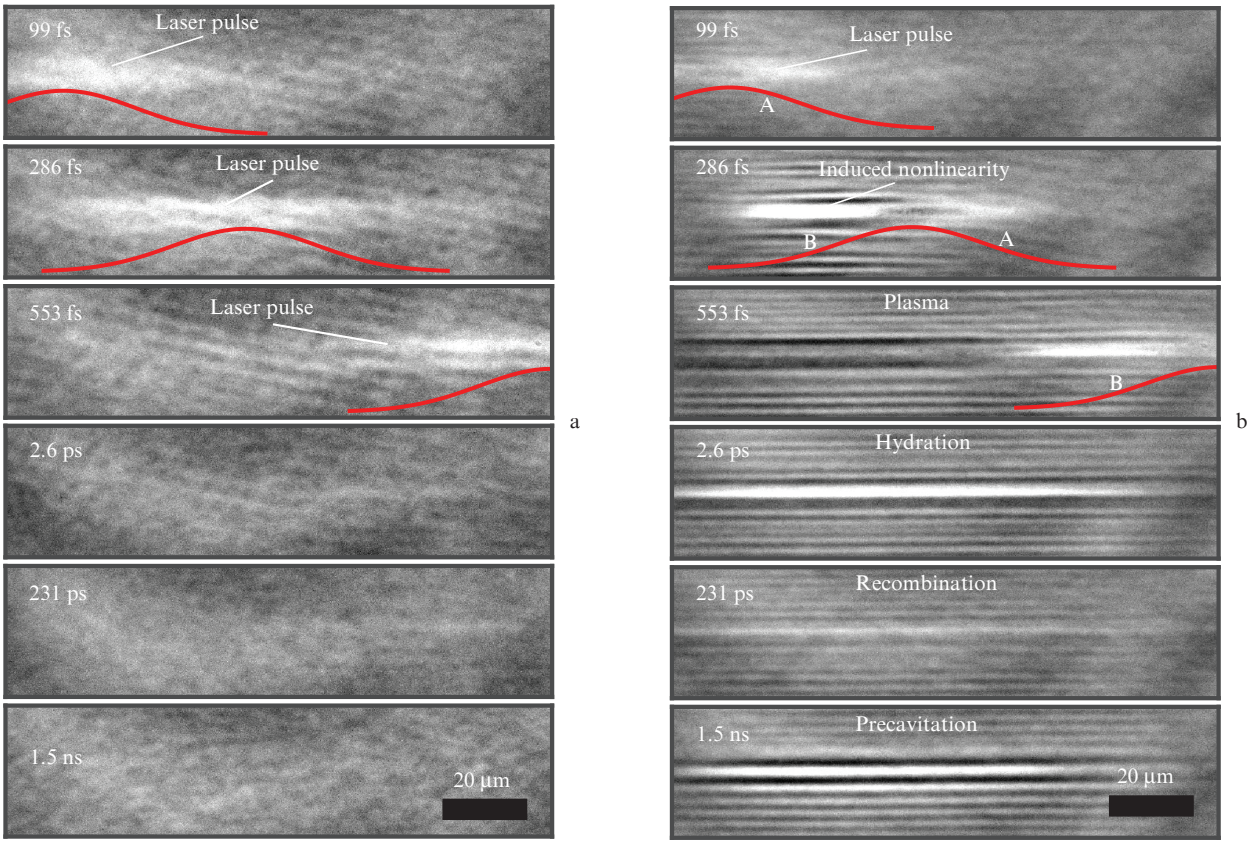

Figure 2. Phase images demonstrating the evolution of a laser-excited region in water at pulse energies E = (a) 0.26 and (b) 0.4 μJ; the pulse propagates from left to right. The probe-pulse delay is indicated in each image. The pulse position at a given delay is shown by continuous curves. The leading and trailing parts of pulse are denoted as A and B, respectively.

with a speed of light. This short-term (less than 1 ps) dynamics was described in detail in [25], where it was suggested that the observed rise in polarisability in the end of the pulse is related to the nonlinear optical properties of excited carriers.

At a delay of 553 fs the trailing part was still in the field of view. It can be seen that the Δn value was close to zero after the pulse passage. However, it rapidly increased with time and reached a local maximum after ~2 ps (Fig. 2, 2.6-ps delay). This rise is caused by the solvation of carriers, which leads to a shift of the absorption band to the range near 720 nm and a corresponding change in the polarisability sign. Then, the water polarisability gradually (nonexponentially) decreased. After 100–200 ps, the Δn value reached again a minimum (Fig. 2, 231-ps delay) and then started increasing again.

This rise was linear in time and continued for at least 1.5 ns, which is the maximally possible delay for the experimental setup (Fig. 2, 1.5-ns delay). The formation of a region with enhanced polarisability was observed on the nanosecond time scale every time when solvated plasma was detected. A strict correlation was observed: the larger the Δn value on the picosecond scale, the larger this quantity on the nanosecond scale.

The occurrence of gas bubbles was detected 1 ms after the impact by the next pulse in a train at a repetition rate of 1 kHz. The corresponding shadow photographs are presented in Fig. 3.

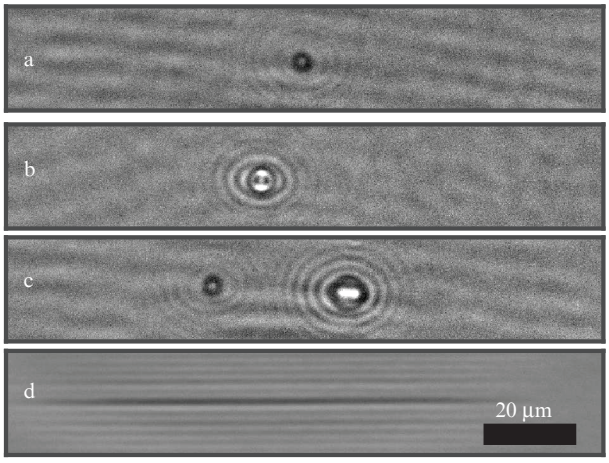

Figure 3. Shadow images obtained 1 ms after the laser impact, which demonstrate the formation of gas bubbles at pulse energies of (a) 0.29, (b) 0.38, and (c) 0.52 μJ; (d) shadow photograph of the plasma obtained at a delay of 2 ps and energy of 0.38 μJ (corresponds to panel b).

The bubble formation began with certain threshold energy (~0.25 μJ under given irradiation conditions) and was expectedly localised at the point of maximum plasma concentration (compare Figs 3b and 3d). An increase in impact energy led to an increase in the diameters of bubbles and then to their multiple generation within one pulse.

In the case of hexane the dynamics of induced optical polarisability was significantly different. The phase images demonstrating the corresponding changes for hexane are shown in Fig. 4. The delays between the probe and pump pulses in Figs 2 and 4 are almost the same. It can be seen that the optical changes induced by excited plasma in hexane are much smaller than those induced in water. At the instants when the wave packet was in the caustic, a zone with minimal changes in the refractive index manifested itself against the background of Kerr hyperpolarisability [Fig. 4, (99–533)-fs delays]. The $\Delta\phi$ value in this zone did not exceed the noise level, in view of which the sign of change could not be reliably determined.

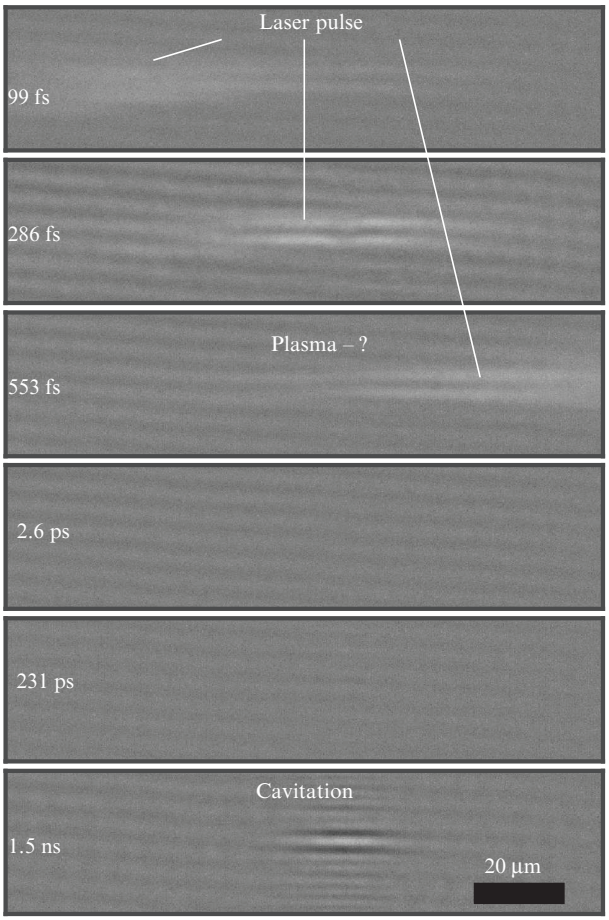

Figure 4. Phase images demonstrating the evolution of laser-excited region in hexane at a pulse energy $E = 0.2$ μJ; the pulse propagates from left to right. The probe-pulse delay is indicated in each image.

After the pulse passed through the caustic, the aforementioned zone was not visualised: the changes Δn and ΔA were close to zero (i.e., below the sensitivity threshold of the system in use). Thus, in the case of hexane irradiation, neither formation, nor solvation, nor recombination of plasma was observed. At a delay of ~200 ps the refractive index of hexane began to rise, as well as that of water. As in water, this rise lasted for at least 1.5 ns. In this case, the thresholds of bubble formation in the impact zone for water and hexane were, respectively, ~0.25 and ~0.1 μJ.

The dynamics of changes in the optical properties of liquids under study are presented in Fig. 5. The post-pulse evolution of the optical properties of water was analysed in detail in [26], where the characteristic time of carrier solvation ($\tau_{sol} \approx 1000$ fs) and electron–ion recombination were determined. It was shown that, upon excitation at a wavelength of 800 nm, the kinetics of the latter process is described by a temporal dependence in the form $\sqrt{\tau_j/t}$, which arises if this process is considered as an attachment of the electron to the

parent cation as a result of their collision after a series of diffuse jumps [27]. The reported data for water were used to determine the time of a single jump in the diffuse motion of charges toward each other: $\tau_j \approx 500$ fs. Here, we are interested to a greater extent in the mechanisms of light energy dissipation in water and hexane.

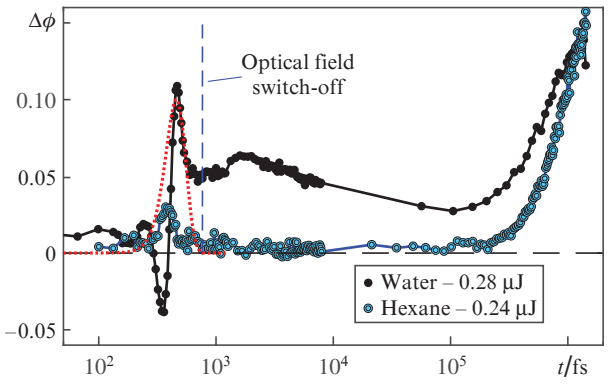

Figure 5. (Colour online) Dynamics of induced changes in polarisability for water and hexane. The probe-beam phase shift (λ = 800 nm) is measured at the centre of the impact zone. The dotted line corresponds to the autocorrelation function of 165-fs laser pulse.

The concentrations of carriers, both excited and solvated in water, were estimated from the data on absorption dynamics. The maximum optical density A_w in the laser impact zone was fixed 1 ps after the pulse transmission and turned out to be as high as ~0.05. Proceeding from the known value of molar extinction coefficient (ϵ_w = 22700 M^{-1} cm^{-1} [28]), the concentration of solvated electrons was about 5×10^{18} cm^{-3}. Comparable concentrations were obtained in [9] [$(1-2)\times10^{19}$ cm^{-3}] and [29] (3×10^{19} cm^{-3}). Note that theoretical calculations give close values in the case of multiphoton absorption during ionisation. With allowance for the shock ionisation, the free-carrier concentration increases by two orders of magnitude [30].

It is more difficult to obtain the corresponding estimates for hexane, because there are no reliable data on the optical absorption of excited carriers. According to indirect estimations based on calorimetric and spectral measurements of some other alkanes, the molar extinction $\epsilon_a \approx 800-1800$ M L cm^{-1} [31]. Based on this, one can estimate from above the concentration of laser-induced carriers in the above-described experiments. Since the optical density A_h of hexane did not exceed ~0.001 (noise level) during irradiation, the carrier concentration in it was below $(1.5-3.0)\times10^{18}$ cm^{-3}; i.e., the concentrations of radiation-excited carriers in water and hexane are apparently on the same order of magnitude. The observed cavitation intensities under these conditions are expectedly close. However, in both cases the obtained carrier concentration is too low to initiate heating sufficient for cavitation development.

Cavitation as a phenomenon in which phase transitions are due to fast and local liquid heating, begins after the recombination of induced plasma, when the energy of electron subsystem is transformed into thermal motion of liquid molecules. The observed dynamics (Fig. 5) confirms this point of view; nevertheless, some important questions arise.

Simple estimations show that, at the observed plasma density of $\sim10^{19}$ cm^{-3}, the energy dissipation from each electron (~6.5 eV in case of water) provides heating by no more than ~3 K. It was suggested [18] that the temperature must be increased by ~150 K to initiate cavitation. One might expect that nonlinear absorption provides only a relatively small number of seeding delocalised carriers, and the main channel of radiation energy transfer to the liquid is related to the linear absorption of light by these presolvated electrons. In this case either an electron avalanche develops, or the concentration of carriers remains limited but their temperature should become sufficiently high (much larger than 10 eV). Note that the chain of processes occurring in liquids, from radiation absorption to cavitation, was calculated within this suggestion. The calculation results showed that cavitation may develop at impact energies used in experiments [18, 32]. However, there are questions still to be answered. Indeed, if avalanche multiplication of carriers is implemented, why cannot the produced plasma be seen in the interference patterns and shadow images? On the other hand, if hot carriers are not multiplied in the IR field, being heated to high temperatures, it is unclear why the observed recombination corresponds to the case of cold electrons, whose energy is too low to overcome the Onsager sphere [33] and leave the parent ion vicinity. In our opinion, this contradiction can be resolved only in terms of mechanisms of energy transfer from carriers to vibrations of liquid molecules for times comparable with the pulse duration (100 fs or shorter). These mechanisms and their contribution to the dissipation processes are being studied now [17].

4. Conclusions

Our experiments made it possible to trace the dynamics of the optical properties of pure water and hexane in the zone impacted by focused femtosecond pulses with an intensity of $\sim10^{13}$ W cm^{-2}. It was demonstrated that the recombination of solvated plasma and cavitation in both liquids are independent processes, evolving successively on pico- and nanosecond time scales. The solvation and recombination times are in good agreement with the data of other studies [15, 17, 27].

The concentration of carriers excited by a femtosecond pulse in the cavitation regime was found to be less than 10^{19} cm^{-3}. In this case, the electron–ion recombination occurs according to the diffusion geminal mechanism, when a delocalised electron cannot leave the parent cation. The plasma temperature should be relatively low under these conditions. At the same time, the above-described measurements were performed in the cavitation regimes; i.e., the laser-induced plasma with a relatively low concentration causes a significant rise in temperature in the impacted microvolume of the liquid. Thus, our experiments put new questions about the mechanisms of energy transfer under intense laser irradiation of both polar and nonpolar liquids. To resolve the observed contradictions, it is necessary to study more comprehensively the processes of transformation of excited-carrier energy into the vibrational energy of liquid molecules.

Acknowledgements. This work was supported by the Russian Science Foundation (Grant No. 19-12-00255).

References

1. Halbout J.M., Tang C. *Appl. Phys. Lett.*, **40**, 765 (1982).
2. Siders C., Le Blanc S., Fisher D., Tajima T., Downer M., Babine A., Stepanov A., Sergeev A. *Phys. Rev. Lett.*, **76**, 3570 (1996).

3. Guizard S., D'Oliveira P., Daguzan P., Martin P. *Nucl. Instrum. Meth. Phys. Res. Sec. B*, **116**, 43 (1996).
4. Schmidt V., Husinsky W., Betz G. *Phys. Rev. Lett*., **85**, 3516 (2000).
5. Chien C., La Fontaine B., Desparois A., Jiang Z., Johnston T., Kieffer J., Pépin H., Vidal F., Mercure H. *Opt. Lett.*, **25**, 578 (2000).
6. Temnov V.V., Sokolowski-Tinten K., Zhou P., von der Linde D. *Appl. Phys. A*, **78**, 483 (2004).
7. Guizard S., Klimentov S., Mouskeftaras A., Fedorov N., Geoffroy G., Vilmart G. *Appl. Surf. Sci*., **336**, 206 (2014).
8. Teslenko B. *Sov. J. Quantum Eelectron.*, **5**, 676 (1975) [*Kvantovaya Elektron*., **2**, 1248 (1975)].
9. Sarpe C., Köhler J., Winkler T., Wollenhaupt M., Baumert T. *New J. Phys*., **14**, 075021 (2012).
10. Palianov P., Quéré F., Pommeret S. *J. Experiment.Theoret. Phys*., **118**, 489 (2014).
11. Migus A., Gauduel Y., Martin J.L., Antonetti A. *Phys. Rev. Lett*., **58**, 1559 (1987).
12. Long F.H., Lu H., Eisenthal K.B. *Phys. Rev. Lett*., **64**, 1469 (1990).
13. Silva C., Walhout P.K., Yokoyama K., Barbara P.F. *Phys. Rev. Lett*., **80**, 1086 (1998).
14. Laenen R., Roth T., Laubereau A. *Phys. Rev. Lett*., **85**, 50 (2000).
15. Pshenichnikov M.S., Baltuška A., Wiersma D.A. *Chem. Phys. Lett*., **389**, 171 (2004).
16. Zho C., Schwartz B.J. *J. Phys. Chem. B*, **120**, 12604 (2016).
17. Karashima S., Yamamoto Y., Suzuki T. *J. Phys. Chem. Lett.*, **10**, 4499 (2019).
18. Vogel A., Noack J., Hüttman G., Paltauf G. *Appl. Phys. B*, **81**, 1015 (2005).
19. Wesolowski M.J., Kuzmin S., Moores B., Wales B., Karimi R., Zaidi A.A., Leonenko Z., Sanderson J.H., Duley W.W. *Carbon*, **49**, 625 (2011).
20. Kanjana K., Courtin B., MacConnell A., Bartels D.M. *J. Phys. Chem. A*, **119**, 11094 (2015).
21. Gruzdev V., Korkin D., Mooney B.P., Havelund J.F., Müller I.M., Thelen J. *J. Sci. Rep.*, **7**, 5550 (2017).
22. Stein G. *Discuss. Faraday Soc*., **12**, 227 (1952).
23. Schaffer C., Nishimura N., Glezer E., Kim A., Mazur E. *Opt. Express*, **10**, 196 (2002).
24. Zavedeev E.V., Kononenko V.V., Konov V.I. *Appl. Phys. A*, **123**, 499 (2017).
25. Kononenko V.V., Gololobov V.M., Konov V.I. *Opt. Lett*., **45**, 256 (2020).
26. Kononenko V.V., Gololobov V.M., Zavedeev E.V., Konov V.I. *JOSA B*, **37**, 2615 (2020).
27. Shank C., Yen R., Fork R., Orenstein J., Baker G. *Phys. Rev. Lett*., **49**, 1660 (1982).
28. Hare P.M., Price E.A., Bartels D.M. *J. Phys. Chem. A*, **112**, 6800 (2008).
29. Minardi S., Milián C., Majus D., Gopal A., Tamošauskas G., Couairon A., Pertsch T., Dubietis A. *Appl. Phys. Lett*., **105**, 224104 (2014).
30. Linz N., Freidank S., Liang X., Vogel A. *Phys. Rev. B*, **94**, 024113 (2016).
31. Morais J., Zimmt M.B. *J. Phys. Chem.*, **99**, 8863 (1995).
32. Linz N., Freidank S., Liang X., Vogelmann H., Trickl T., Vogel A. *Phys. Rev. B*, **91**, 134114 (2015).
33. Lu H., Long F.H., Eisenthal K. *J. Opt. Soc. Am. B*, **7**, 1511 (1990).